

RESEARCH ARTICLE

10.1002/2017JD027143

Key Points:

- The measured rate of meteoric smoke deposition and the mesospheric fluxes of Na and Fe are not reconciled in a whole atmosphere model
- The approximately fivefold higher smoke deposition flux in central Greenland, compared with eastern Antarctica, is not captured by the model
- Sensitivity experiments with the model deposition scheme, and use of an alternative global model, do not significantly improve agreement

Supporting Information:

- Data Set S1
- Data Set S2
- Figure S1

Correspondence to:

J. M. C. Plane,
j.m.c.plane@leeds.ac.uk

Citation:

Brooke, J. S. A., Feng, W., Carrillo-Sánchez, J. D., Mann, G. W., James, A. D., Bardeen, C. G., & Plane, J. M. C. (2017). Meteoric smoke deposition in the polar regions: A comparison of measurements with global atmospheric models. *Journal of Geophysical Research: Atmospheres*, 122, 11,112–11,130. <https://doi.org/10.1002/2017JD027143>

Received 16 MAY 2017

Accepted 8 SEP 2017

Accepted article online 14 SEP 2017

Published online 16 OCT 2017

Meteoric Smoke Deposition in the Polar Regions: A Comparison of Measurements With Global Atmospheric Models

James S. A. Brooke¹ , Wuhu Feng^{1,2} , Juan Diego Carrillo-Sánchez¹ , Graham W. Mann² , Alexander D. James¹ , Charles G. Bardeen³ , and John M. C. Plane¹ 

¹School of Chemistry, University of Leeds, Leeds, UK, ²National Centre for Atmospheric Science, School of Earth and Environment, University of Leeds, Leeds, UK, ³Atmospheric Chemistry Observations and Modeling Laboratory, National Center for Atmospheric Research, Boulder, CO, USA

Abstract The accumulation rate of meteoric smoke particles (MSPs) in ice cores—determined from the trace elements Ir and Pt, and superparamagnetic Fe particles—is significantly higher than expected from the measured vertical fluxes of Na and Fe atoms in the upper mesosphere and the surface deposition of cosmic spherules. The Whole Atmosphere Community Climate Model with the Community Aerosol and Radiation Model for Atmospheres has been used to simulate MSP production, transport, and deposition, using a global MSP input of 7.9 t d^{-1} based on these other measurements. The modeled MSP deposition rates are smaller than the measurements by factors of ~ 32 in Greenland and ~ 12 in Antarctica, even after reanalysis of the Ir/Pt ice core data with inclusion of a volcanic source. Variations of the model deposition scheme and use of the United Kingdom Chemistry and Aerosols model do not improve the agreement. Direct removal of MSP-nucleated polar stratospheric cloud particles to the surface gives much better agreement, but would result in an unfeasibly high rate of nitrate deposition. The unablated fraction of cosmic dust ($\sim 35 \text{ t d}^{-1}$) would provide sufficient Ir and Pt to account for the Antarctic measurements, but the relatively small flux of these large ($>3 \mu\text{m}$) particles would lead to greater variability in the ice core measurements than is observed, although this would be partly offset if significant fragmentation of cosmic dust particles occurred during atmospheric entry. Future directions to resolve these discrepancies between models and measurements are also discussed.

Plain Language Summary About 40 t of space dust enters the atmosphere every day. Around 20% of the dust vaporizes during entry because the particles enter at speeds of over 40,000 kph. The resulting metal vapors (principally Fe, Mg, and Si) then oxidize and condense into tiny particles known as meteoric smoke, around 1 nm in radius. This study examines where the meteoric smoke is deposited at the Earth's surface. The smoke has been detected in polar ice cores, with a much higher deposition rate than expected from measurements in the upper atmosphere. A global circulation model was therefore used to analyze how the smoke is transported from around 80 km altitude and deposited in Greenland and Antarctica, mainly by snow. The model cannot satisfactorily account for either the absolute rate of deposition or the ratio of the deposition rates in the polar regions. A variety of explanations to account for this discrepancy are then explored, including a volcanic artifact in the ice cores, fragmentation of meteoroids, and a temporal change in the cosmic dust input.

1. Introduction

The ablation of cosmic dust in the Earth's upper atmosphere results in the presence of layers of metal atoms between about 80 and 105 km (Plane et al., 2015). Below 80 km these metals are converted into compounds such as oxides, hydroxides, and carbonates, which polymerize to form nanometer-sized meteoric smoke particles (MSPs) (Saunders & Plane, 2006). MSPs are likely to be composed of Fe, Mg, Si, and O, probably in the form of olivines ($\text{Fe}_x\text{Mg}_{2-x}\text{SiO}_4$, $0 \leq x \leq 2$) or pyroxenes ($\text{Fe}_x\text{Mg}_{1-x}\text{SiO}_3$, $0 \leq x \leq 1$) (Hervig et al., 2012; Plane et al., 2015). MSPs are transported first by atmospheric circulation to the stratosphere, then by a combination of circulation and sedimentation, to be ultimately deposited at the surface after an average of 4–5 years (Dhomse et al., 2013).

Estimates of the total atmospheric input of cosmic dust have varied between around 3 and 300 t d^{-1} (Plane, 2012). Methods used to determine the input have included the Long Duration Exposure Facility

(LDEF), which detected dust in low Earth orbit (Love & Brownlee, 1993), meteor radars (Hughes, 1978; Mathews et al., 2001), and lidar measurements of the vertical fluxes of Na and Fe atoms in the upper mesosphere (Gardner et al., 2014; Gardner et al., 2016; Huang et al., 2015). There have also been many estimates of the dust input from the surface deposition of micrometeorites and cosmic spherules (melted micrometeorites that did not fully ablate during atmospheric entry), using measurements of Ir (e.g., Karner et al., 2003; Kyte & Wasson, 1986), Os (e.g., Esser & Turekian, 1993; Peucker-Ehrenbrink & Ravizza, 2000) and ^3He (e.g., Brook et al., 2000; Marcantonio et al., 1999; Winckler & Fischer, 2006) in ocean sediments, and cosmic spherule counts (e.g., Maurette et al., 1986; Prasad et al., 2013; Taylor et al., 1998). These and other measurements have been compared and tabulated by Karner et al. (2003), Plane (2012), and Prasad et al. (2013). Surface deposition studies have provided measurements of the total dust input rate or the flux of micrometeorites (typically much larger than $1\ \mu\text{m}$) that have survived entry. However, they do not provide measurements of the ablation flux, which should be exclusively represented by the much smaller MSPs.

The first reported detection of MSP surface deposition was by Gabrielli et al. (2004), who measured Ir and Pt in ice core samples from the Greenland Ice Core Project (GRIP) at Summit, central Greenland (72°N , 38°W) (Dansgaard et al., 1993). These siderophile elements are significantly enriched in cosmic dust with respect to the Earth's crust (Barker & Anders, 1968; Ganapathy et al., 1978). The method of dissolving the ice core extract in weak nitric acid, followed by inductively coupled plasma ionization and detection by mass spectrometry, was designed to exclude most Ir and Pt from larger ($r > 200\ \text{nm}$) particles. Significant enrichment of both Ir and Pt with respect to Al (a proxy for crustal dust) was found during the Holocene, with an average Ir/Pt ratio close to the chondritic ratio of 0.49 (Asplund et al., 2009), and so the Ir and Pt signals were ascribed to MSPs. During the Last Glacial Age (LGA), the MSP signal was obscured by the much higher loading of terrestrial crustal dust. Assuming a chondritic composition, 100% ablation (i.e., all the incoming Ir and Pt evaporated and then became incorporated into MSPs), and uniform global deposition, the cosmic dust input during the Holocene was estimated to be $214 \pm 82\ \text{t d}^{-1}$. Since this is a relatively high value (Plane, 2012), Gabrielli et al. (2004) suggested that MSP deposition might be enhanced in the polar regions as a result of the prevailing mesospheric meridional transport to the winter pole, followed by descent in the winter polar vortex.

A similar ice core study was then performed by Gabrielli et al. (2006) at two sites in Antarctica: the European Project for Ice Coring in Antarctica (EPICA) at Dome C (75°S , 123°E) (Augustin et al., 2004) and at Vostok (78°S , 107°E) (Petit et al., 1999). Surprisingly, higher Pt and Ir concentrations were observed at both sites during interglacial periods, despite lower atmospheric dust concentrations. This was attributed to a weaker interglacial polar vortex, which allowed more in-land transport of Ir- and Pt-enriched volcanic emissions. Thus, the cosmic dust flux during these interglacial periods could not be determined, but global inputs of 56 ± 22 and $64 \pm 26\ \text{t d}^{-1}$ were calculated during glacial periods at Vostok and EPICA, respectively.

MSP fluxes have also been reported from observations of superparamagnetic Fe in ice cores, at the North Greenland Ice Core Project (NGRIP; 75°N , 42°W) (Lanci, 2004; Lanci & Kent, 2006), EPICA (Lanci et al., 2008), and Vostok (Lanci et al., 2007). These studies were subsequently summarized by Lanci et al. (2012). At each site, for a set of time-varying samples, the isothermal remnant magnetization (IRM) was measured at 77 K, and then again at 255 K; a decrease in magnetization was observed following heating. The magnetization remaining at 255 K is referred to as the stable magnetization, and the magnetization lost between 77 and 255 K is the superparamagnetic (SP) fraction. This SP fraction was assigned to particles with radii between 4 and 10 nm, which were assumed to be MSPs. The concentrations of crustal dust with radius $> 0.1\ \mu\text{m}$ were also measured, and the SP fraction was plotted against this concentration. Crustal dust may also contain a fraction of small particles which are SP, but it was assumed that at zero concentration of measurable crustal dust (i.e., particles with $r > 0.1\ \mu\text{m}$), there was also no terrestrial SP component. Therefore, the intercept of SP magnetization against crustal dust ($r > 0.1\ \mu\text{m}$) represents the magnetization caused by MSPs. This was converted to an Fe concentration assuming magnetite composition (see section 4.5), from which a global MSP input rate was calculated assuming uniform global deposition. Using the Fe concentrations for all three sites reported in Lanci et al. (2012), and snow accumulation rates of 17.4, 2.5, and $2.0\ \text{g cm}^{-2}\ \text{yr}^{-1}$, for NGRIP, EPICA, and Vostok, respectively (Andersen et al., 2004; Lanci et al., 2012), and a recent estimate of the Fe content of MSPs of 33% (Carrillo-Sánchez et al., 2016), leads to MSP input rates of 129 ± 18 , 17 ± 2.5 , and $21 \pm 7\ \text{t d}^{-1}$ for

NGRIP, Vostok, and EPICA, respectively. These values are a factor of between 1.7 and 3.3 times smaller than the Ir/Pt estimates discussed above.

Recently, Carrillo-Sánchez et al. (2016) used the cosmic spherule accretion rate at the bottom of an ice chamber at the Amundsen-Scott base at South Pole (Taylor et al., 1998), together with recent measurements of the vertical fluxes of Na and Fe atoms above 87 km in the atmosphere (Gardner et al., 2014; Gardner et al., 2016; Huang et al., 2015), to determine the total cosmic dust input mass to be $43 \pm 14 \text{ t d}^{-1}$, of which $80 \pm 17\%$ came from Jupiter Family Comets. Since the average entry velocity of the particles from these short-period comets is around 14 km s^{-1} (Carrillo-Sánchez et al., 2015), only $7.9 \pm 2.6 \text{ t d}^{-1}$ ablates, i.e. $\sim 18\%$ of the total input. Because the bulk mineral in cosmic dust is olivinic with similar elemental abundances of Fe, Mg, and Si (Asplund et al., 2009), and these elements should then oxidize and form MSPs, the total mass of MSPs injected into the atmosphere should be similar to the ablated mass, i.e. $\sim 8 \text{ t d}^{-1}$.

MSP deposition has previously been modeled by Dhomse et al. (2013) using a simple formalism to estimate the rate of wet MSP deposition in the UK's Unified Model (UM). This approach was based on the observation by Lanci et al. (2012) that the MSP deposition rate correlated with snowfall, and hence, wet appeared to be much more important than dry deposition. Dhomse et al. (2013) obtained a Greenland/Antarctica deposition ratio of about 15 (somewhat higher than the ratio of ~ 7 based on both the Ir/Pt and superparamagnetic Fe fluxes discussed above). The global MSP input rate used by Dhomse et al. (2013) was 27 t d^{-1} , i.e. a factor of 3.4 times larger than the most recent estimate of 7.9 t d^{-1} from Carrillo-Sánchez et al. (2016). Scaling the Dhomse et al. (2013) model results to this smaller input rate indicates that the UM study underpredicted the MSP deposition by factors of ~ 6.6 and 15 in Greenland and Antarctica, respectively.

In this paper we report a more detailed modeling study of MSP transport in the atmosphere and deposition at the surface, using a Whole Atmosphere Community Climate Model (WACCM) coupled to an aerosol microphysics model (Community Aerosol and Radiation Model for Atmospheres (CARMA)). The simulations resolve growth of MSPs through coagulation above 35 km, and also, following descent into the Junge layer, growth via uptake of sulfuric acid and water. To assess whether our findings are specific to WACCM-CARMA, we also carry out equivalent simulations with a different global composition-climate model (UM-United Kingdom Chemistry and Aerosols (UKCA); see section 2.5), which has finer vertical resolution and a modal aerosol microphysics scheme (GLOMAP, where aerosol concentrations are recorded in a few modes represented by lognormal distributions, and for each mode only the number and mass concentration values need to be tracked (Mann et al., 2010)), as opposed to the sectional scheme (where mass or number concentrations are tracked for multiple different size bins) used in CARMA.

2. Model Description

2.1. WACCM-CARMA

WACCM is a 3-D numerical high-top coupled chemistry-climate model extending vertically from the surface to about 140 km (e.g., Marsh et al., 2013), which is part of the National Center for Atmospheric Research's Community Earth System Model (CESM) (Hurrell et al., 2013). In this study, CESM v1.2.2 and WACCM 4 (CAM v5.3.57) were used. Aerosol properties are computed using CARMA, which employs a sectional (size bin) representation. Specified dynamics was used for all the WACCM runs, with meteorological values nudged below 50 km using the Modern-Era Retrospective Analysis for Research and Applications (MERRA) reanalysis (Rienecker et al., 2011). This means that uncertainties remain in the vertical transport above 50 km, which could be resolved in the future using WACCM with a reanalysis extending from the surface to the lower thermosphere (Pedatella et al., 2013, 2014).

WACCM includes a detailed neutral chemistry for the middle atmosphere based on the Model for Ozone and Related Chemical Tracers (MOZART) (Kinnison et al., 2007) and sulfur chemistry from English et al. (2011); there are 66 species, including the sulfur-containing species OCS, S, SO, SO₂, SO₃, HSO₃, H₂SO₄, and a large set of photolysis, gas phase, and heterogeneous reactions, as in Lamarque et al. (2012). Natural and anthropogenic emissions of SO₂, NO₂, NO, CO, NO, and DMS, and boundary conditions including for OCS were included as in Lamarque et al. (2012). SO₂ emissions from both continuous quiescent volcanic degassing and explosively erupting volcanoes were also included (Mills et al., 2016). H₂SO₄ visible photolysis rates are from Feierabend et al. (2006), including the pressure dependence from Miller et al. (2007), and Lyman α

Table 1
List of WACCM-CARMA Runs With a Brief Description

Model run	Description
<i>stnd-44</i>	Standard run with 44 t d ⁻¹ MSP input
<i>stnd-7.9</i>	Standard run with 7.9 t d ⁻¹ MSP input
<i>sep-7.9</i>	Standard run but with no interaction between MSP and sulfate
<i>psc-evp-7.9</i>	PSCs precipitating MSPs into upper troposphere, then releasing MSPs
<i>psc-srf-7.9</i>	PSCs precipitating MSPs directly to surface
<i>stnd-7.9-dry</i>	Standard run with increased dry deposition over land
<i>psc-evp-7.9-dry</i>	Run <i>psc-evp-7.9</i> with increased dry deposition over land
<i>unab-43</i>	35.4 t d ⁻¹ unablated large (>3.8 μm) cosmic dust particles, plus 7.9 t d ⁻¹ MSP
<i>impc-7.9</i>	Parameterization of snow impaction scavenging

rates from Lane and Kjaergaard (2008). Additional reactions for DMS have been added to this set—the full list is available in Data Set S1 in the supporting information. The aerosol surface area densities required to calculate the rates of heterogeneous reactions are obtained from CARMA. All simulations were performed on a 2.5° × 1.9° longitude/latitude grid with 88 model levels up to ~140 km and CAM4 physics.

The CARMA aerosols here include two “groups”: pure sulfate and mixed sulfate, where mixed sulfate consists of sulfate with an MSP core. Both groups have 28 bins between 0.34 nm and 1.6 μm, with particle densities of 2.0 and 1.9 g cm⁻³ for pure sulfate and mixed sulfate, respectively. Pure sulfate is formed in the smallest size bin by homogeneous nucleation of H₂SO₄ and H₂O. MSPs are injected into the smallest size bin of the mixed sulfate group (so that they begin as 100% MSP core), using the production rate profile between

75 and 110 km from Kalashnikova et al. (2000), with the input scaled to a selected global input rate from meteoric ablation.

Condensation and evaporation of H₂SO₄ occur for both aerosol groups, but evaporation from mixed sulfate only occurs for particles that have a core fraction less than 0.5. For mixed sulfate, this condensation and limited evaporation mimics the reaction between H₂SO₄ and MSP metal atoms (Saunders et al., 2012). Coagulation occurs within and between both aerosol groups. These microphysical processes are calculated as described by English et al. (2012).

2.2. Standard Aerosol Deposition

The dry deposition rate is calculated within CARMA. The deposition velocity in the lowest grid box is estimated using sedimentation velocities (for all aerosol sizes) and the parameterizations from Zhang and Brook (2001), with land and ocean fractions from WACCM. For a single column, sedimentation velocities are also calculated for all grid boxes above the lowest box. These are used to determine the change in concentration for each box over a time step, and the total change for the column is then the dry deposition flux.

Wet deposition is calculated within CAM, and includes both in-cloud (nucleation) and below-cloud (impaction) scavenging. For each model grid box and aerosol bin, the in-cloud scavenging for both convective and stratiform precipitation is calculated as

$$T_{IC} = c_{sol} f_c f_p q, \quad (1)$$

where T_{IC} is the change in aerosol concentration (tendency; in kg m⁻³ s⁻¹), c_{sol} is a solubility factor between 0 and 1 (there is no difference in the treatment of water and ice scavenging), f_c is the fraction of the box covered by cloud, f_p is the fractional rate at which cloud water is converted to precipitation (s⁻¹), and q is the tracer concentration (in kg m⁻³). In the troposphere the overwhelming majority of the aerosol mass is sulfate (e.g., in the standard model run, *stnd-7.9* (see Table 1), 0.004% by mass is MSP), and all MSPs are expected to be within sulfate particles, so a solubility factor of 1 is used.

Aerosol concentration tendencies due to below-cloud scavenging are obtained as

$$T_{BC} = c_{sol} c_{scv} p q \quad (2)$$

where p is the precipitation rate (in kg m⁻² s⁻¹) and c_{scv} is the impaction scavenging coefficient which is set to 0.1 mm⁻¹ (or m² kg⁻¹ of water) for all aerosol types and sizes, and the same solubility factor of 1 as above.

Each aerosol bin is processed as a column, starting at the top, and aerosol scavenged in stratiform precipitation is released into lower grid boxes if evaporation of the precipitation occurs. For convective precipitation, the aerosol is removed directly to the surface.

2.3. Model Runs and Variations From the Standard Version

Table 1 contains the name and brief description of each model run, where the number in the model run name is the cosmic dust input used (in t d⁻¹). The *stnd-7.9* runs thus have an input of 7.9 t d⁻¹ based on Carrillo-Sánchez et al. (2016), and the *stnd-44* runs have an input of 44 t d⁻¹, based on an old estimate from

Hughes (1978) and previously used in a WACCM-CARMA study of MSPs in the middle atmosphere (Bardeen et al., 2008).

Two runs used a different scheme to that described in section 2.1. Run *sep-7.9* used pure MSP and pure sulfate groups only, with no interaction between them, in order to assess the effect of including the MSP-sulfate interaction. Run *unab-43* extends the size bins by 20 so that the maximum radius is over 500 μm . 35.4 t d^{-1} of unablated dust (including cosmic spherules) with radii between 3.8 and 500 μm can then be included, based on the recent results from Carrillo-Sánchez et al. (2016) (size distribution in Figure S1 in the supporting information). For this run, the standard 7.9 t d^{-1} of MSP was also included.

Nucleation of polar stratospheric clouds (PSCs) has been proposed to occur on MSPs (Voigt et al., 2005). If the resulting nitric acid-trihydrate (NAT) particles grow large enough, they can precipitate through the tropopause. Two runs were performed to simulate the potential effects of PSC precipitation (section 3.3). The first represents an upper limit, in which 90% of the aerosol in a grid box precipitates directly to the surface after PSC formation (*psc-srf-7.9*). In the second run the NAT particles precipitate through the tropopause and MSPs are released below 400 hPa (*psc-evp-7.9*), which simulates the complete evaporation of NAT particles after entering the troposphere. PSC formation was modeled to occur if the temperature fell below 194 K, at pressure levels between 10 and 400 hPa ($\sim 7\text{--}27 \text{ km}$). This is approximately 4 K below the temperature at which NAT becomes thermodynamically stable, a freezing depression which was recently shown to produce a good match to observed clouds (Hoyle et al., 2013). A more detailed implementation of PSC freezing in the model would require a parameterization of heterogeneous nucleation kinetics and NAT growth and sedimentation, which is beyond the scope of this study.

Runs *impc-7.9*, *stnd-7.9-dry*, and *psc-evp-7.9-dry* are described in section S1 in the supporting information.

2.4. Initialization and Time Coverage

Runs *stnd-7.9*, *stnd-44*, and *sep-7.9* begin in January 2001, initialized from a specified dynamics WACCM-CARMA run obtained from the CESM repository. MSP concentrations were initialized separately from a previous free-running 7.9 t d^{-1} WACCM-CARMA run, and scaled linearly for the *stnd-44* run. Runs *psc-evp-7.9* and *psc-srf-7.9* were initialized from the output of *stnd-7.9* in August 2003 to allow an initial spin-up period. These were all continued until November 2014, and 9 year averages from December 2005 to November 2014 are compared in section 3.

The run representing unablated material (*unab-43*) was initialized from the output of *stnd-7.9* in January 2006 and continued until April 2007. Only 1 year of output was required for this run as the larger unablated cosmic dust is not affected significantly by the residual atmospheric circulation.

The remaining five shorter runs were initialized from *stnd-7.9* between January and March 2006, and run until June 2010, with July 2006 to June 2010 averages compared in section 3.

2.5. UM-UKCA

To test whether the MSP deposition results from WACCM-CARMA are also the case for other models, we carried out the standard run also as a parallel experiment in the UM-UKCA composition-climate model (e.g., Morgenstern et al., 2009). The UM-UKCA experiment applied an updated realization of the interactive stratospheric aerosol capability validated by Dhomse et al. (2014), with the model here resolving pure sulfate and mixed MSP-sulfate particles separately as in CARMA. This “version 3 strat-trop” configuration of UM-UKCA is run here in a volcanically quiescent present-day setting, and has also been identically run in a Tambora-perturbed preindustrial setting (Zanchettin et al., 2016). Briefly, MSPs are represented within GLOMAP-mode via the existing accumulation insoluble (acc-ins) mode, which has previously only been applied to transport terrestrial dust (e.g., as in Mann et al., 2010). A key distinction with this new GLOMAP-mode setup is that, whereas previously dust “condensation-aged” from insoluble to soluble modes (at a rate determined by how much soluble material condenses or coagulates onto its surface), in the MSP-extended version this transfer no longer occurs for fine-mode dust. Instead, a new “acc-ins mode sulfate” tracer explicitly tracks how much sulfate is accommodated onto MSPs, and there is no longer any dust in the corresponding accumulation soluble mode.

The top layer of UM-UKCA is at $\sim 85 \text{ km}$, which is around the peak of MSP formation. Therefore, in order to provide a comparable MSP representation, the approach in UM-UKCA is to, above 20 Pa ($\sim 65 \text{ km}$), overwrite

the acc-ins number and mass mixing ratios with zonal average monthly mean MSP concentrations from the WACCM-CARMA simulations. Using this approach, UM-UKCA benefits from the higher model top WACCM (~140 km), while retaining the better resolution of the lower atmosphere in the 85 levels present in UM-UKCA.

The UM-UKCA simulation is a time slice run using repeating year 2000 emissions, sea surface temperatures, and sea ice extent, initialized following over 15 year spin-up with the MSP input included. The 6 years analyzed here were after adjustment from terrestrial dust emissions being switched off, the total burden and deposition then becoming near constant, indicating that the terrestrial dust had all been removed. Since the continual adjustment of the acc-ins GLOMAP tracers in the mesosphere inherently means that it will not match the surface MSP deposition simulated in WACCM-CARMA where the smoke source is provided explicitly, the UKCA deposition (which totaled 2.33 t d^{-1}) was rescaled (increased by a factor of $7.9/2.33$) to match the 7.9 t d^{-1} input deposited in WACCM.

3. Results

WACCM-CARMA provides separate wet and dry deposition fluxes for each aerosol size bin, so these are summed to give the total deposition flux. All of the values reported here for the four polar sites were determined by calculating the total deposition at the midpoints of the surrounding model grid boxes, and linearly interpolating to the exact locations. It should be noted that the difference between the results obtained from the single grid box in which an ice core site is located, and an average of the surrounding grid boxes, was never significant enough to alter any of the conclusions below.

3.1. Standard Run

The deposition fluxes at the ice core locations obtained from the standard *std-7.9* run, which includes an MSP input of 7.9 t d^{-1} , are factors of 33–56 and 11–36 smaller than the observations in Greenland and Antarctica, respectively, as shown in Table 2. With a 7.9 t d^{-1} input, the deposition would need to be very strongly enhanced over the sites with “deposition enhancement ratios” (defined as deposition flux at ice core site/global average) of 16–27 and 2.4–7.6. Figure 1a shows the global distribution of MSP deposition from *std-7.9*, and it can be seen that there is no such enhancement of MSP deposition at the polar locations.

MSPs undergo some stratosphere-troposphere exchange (STE) at high latitudes following polar vortex breakup, but STE mostly occurs at midlatitudes due to tropopause folding caused by storm tracks. The MSPs are then transported poleward in the troposphere, during which significant wet deposition occurs because of relatively high levels of precipitation. This results in the two main deposition bands seen in Figures 1a–1c.

The UKCA run shows a very similar pattern (Figure 1f) of MSP deposition flux distributions as WACCM (Figure 1a) and even lower deposition fluxes at the ice core sites (particularly Greenland). This demonstrates that the general pattern of MSP entrainment into the troposphere and deposition is not specific to WACCM.

3.2. Changes to Deposition Scheme

To assess whether the deposition scheme caused the discrepancy between the ice core measurements and models, runs were performed in which the dry/wet deposition ratio was increased (*std-7.9-dry* and *psc-evp-7.9-dry*), a parameterization for impaction scavenging was used (*imp-7.9*), and wet deposition was turned off completely (*nowet-7.9*). None of these tests affected the deposition fluxes at the ice core sites by more than 35%, which suggests that changes to the deposition scheme are unable to resolve the differences between models and observations. A full description of all of these runs is available in Text S1 in the supporting information.

3.3. PSC-Based Removal of MSPs

The results above suggest that if a large deposition enhancement of MSPs is to be achieved at the ice core locations, MSPs must undergo STE to a much greater extent at higher latitudes. PSCs are thought to be nucleated by MSPs and form in the low temperatures of the lower stratospheric polar vortices (Voigt et al., 2005). Once frozen, PSC particles can grow to radii of 5–10 μm (Carslaw et al., 2002; Fahey et al., 2001; Fueglistaler et al., 2002; Molleker et al., 2014), which is large enough for sedimentation through the tropopause, followed either by evaporation or direct precipitation to the surface.

Table 2
Comparison of MSP Deposition Fluxes at the Ice Core Locations (Bold Type = Measurements)

Year	Input (t d ⁻¹)	Model run/ observation	Flux (g m ⁻² yr ⁻¹) × 10 ^{5a}				Greenland/ Antarctica ratio ^b	Deposition enhancement ratios ^c		Observation (Fe)/model ^d		Observation (Pt/Ir)/model ^e		Revised observation (Pt/Ir)/model ^e	
			NGRIP	GRIP	Vostok	EPICA		Gre. ^b	Ant. ^b	Gre.	Ant.	Gre.	Ant.	Gre.	Ant.
2005 to 2014	(7.9)	Observations (Fe) ^f	9.21	...	1.20	1.48	6.87	16.3	2.4	
	(7.9)	Observations (Ir/Pt) ^g	...	15.4	4.02	4.61	3.57	27.2	7.6	
	(7.9)	Revised observations (Ir/Pt) ^h	...	8.25	...	1.75	4.71	14.6	3.1	
	7.9 ⁱ	Dhomse et al.	...	1.40	0.08	0.11	15.2	2.5	0.16	6.6	14.5	11.0	46.8	5.9	16.2
2006 to 2010	44	std-44	1.56	1.58	0.55	0.77	2.37	0.50	0.21	5.9	2.0	9.8	6.5	5.2	2.3
	7.9	std-7.9	0.28	0.28	0.10	0.14	2.33	0.49	0.21	33.4	11.3	55.7	36.4	29.9	12.7
	7.9	sep-7.9	0.26	0.26	0.10	0.14	2.20	0.47	0.21	35.1	11.2	58.4	36.1	31.3	12.8
	7.9	psc-esp-7.9	2.09	2.38	0.47	0.55	4.38	3.9	0.90	4.4	2.6	6.5	8.5	3.5	3.2
	7.9	psc-srf-7.9	6.00	8.75	1.58	1.39	4.96	13.1	2.6	1.5	0.90	1.8	2.9	0.94	1.3
	7.9	std-7.9 ^j	0.24	0.28	0.10	0.15	2.05	0.46	0.23	38.5	10.5	54.2	33.7	29.0	11.5
2000	7.9	std-7.9-dry	0.26	0.31	0.08	0.10	3.13	0.50	0.16	36.0	14.9	50.1	48.0	26.9	17.8
	7.9	impc-7.9	0.23	0.28	0.11	0.16	1.89	0.45	0.24	39.7	9.9	55.1	31.9	29.5	11.1
	7.9	psc-esp-7.9 ^k	1.01	1.99	0.46	0.63	2.76	2.7	0.96	9.1	2.5	7.7	8.0	4.1	2.8
	7.9	psc-esp-7.9-dry	0.97	1.59	0.46	0.57	2.49	2.3	0.91	9.5	2.6	9.7	8.4	5.2	3.1
	48	unab-43	2.75	2.68	2.75	2.73	0.99	0.79	0.80	3.3	0.49	5.7	1.6	3.1	0.64
	48	UKCA	0.11	0.11	0.11	0.10	1.04	0.19	0.19	83.7	12.7	140	40.9	75.0	17.6

^aUncertainties in the observations have been omitted due to space constraints. Their 1σ values are as follows: 40% for Antarctic Ir/Pt, 38% for Greenland Ir/Pt, 14% for Fe at GRIP, 15% for Fe at Vostok, and 33% for Fe at EPICA. ^bThe Greenland/Antarctica flux ratio, and other columns marked "Gre." or "Ant." are averaged over available sites in Greenland or Antarctica. ^cDeposition enhancement ratios as described in text. For observations, these are the enhancement ratios that would be required to reproduce them with a 7.9 t d⁻¹ MSP input. ^dObserved/calculated fluxes for Fe-derived observations, averaged over available sites. ^eObserved/calculated fluxes for Ir- and Pt-derived observations, averaged over available sites. ^fIr/Pt measurements are taken directly from results reported by Gabrielli et al. (2004) and Gabrielli et al. (2006). Note that the Antarctica measurements are for the LGA and are not expected to be as comparable to present-day models as are those from the Holocene. ^gSee section 1 for a description of the adjustment to the Fe-derived observations. ^hSee section 4.6 for a description. ⁱDhomse et al. (2013) values have been scaled by 7.9/27, as that study used a 27 t d⁻¹ input. ^jValues for the runs *std-7.9*, *psc-esp-7.9*, and *psc-srf-7.9* are calculated for both time periods (2005–2014 and 2006–2010), for correct comparison with other runs in both time periods.

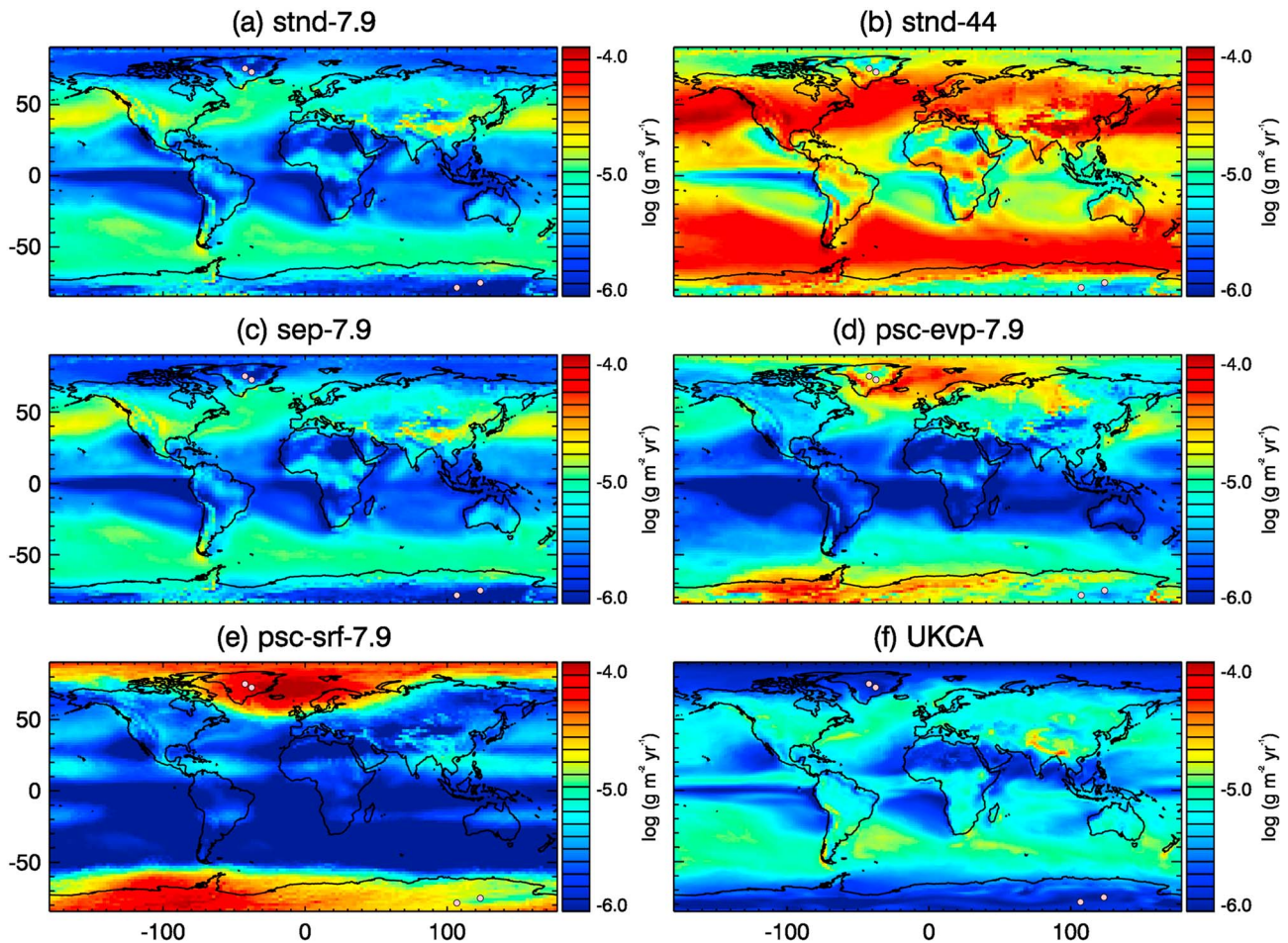


Figure 1. Maps of averaged MSP deposition flux in $\log_{10}(\text{g m}^{-2} \text{yr}^{-1})$. (a–e) WACCM-CARMA runs, 9 years from December 2005 to November 2014. (f) UKCA run, 6 year average (for year 2000). The pink circles indicate the ice core locations.

Two runs, *psc-srf-7.9* and *psc-evp-7.9*, were performed as described in section 2.3, and their deposition patterns are shown in Figures 1d and 1e, respectively. Run *psc-srf-7.9* was designed to represent an upper limit to this PSC removal process, where MSP-containing PSCs are removed directly to the surface. As expected, this does improve the deposition fluxes with regard to the observations, giving the best observed/calculated ratios obtained in this study, of 1.5–1.8 and 0.9–2.9 for Greenland and Antarctica, respectively (Table 2). Unlike *psc-srf-7.9*, run *psc-evp-7.9* (where the PSCs evaporate once in the troposphere) still relies on normal wet/dry deposition after sedimentation across the tropopause has occurred at high latitudes. In this run, the deposition rates at the ice cores sites are approximately double those of the standard *stnd-7.9* run. The atmospheric MSP concentrations—and hence wet deposition—in this run are much higher above the ice core sites than in the other runs (Figure S2). However, the in-cloud wet deposition method described in section 2.2 should represent an upper limit, as it uses a solubility factor of 1.0 and no other scavenging coefficient; hence, increasing it arbitrarily would not be physically reasonable.

3.4. Unablated Cosmic Dust

As unablated cosmic dust is now thought to make up ~82% of the total cosmic dust input (Carrillo-Sánchez et al., 2016), run *unab-43* was performed to include a second fraction of larger unablated particles ($r = 3.8\text{--}500 \mu\text{m}$). Figure S3d shows that, as expected, these relatively large particles sediment rapidly and dry-deposit almost isentropically. The deposition enhancement ratios, including both unablated dust and MSPs, are 0.79 and 0.80 in Greenland and Antarctica, respectively.

4. Discussion

The high level of MSP deposition over Greenland cannot be matched by the current model with global MSP input of 7.9 t d^{-1} , even with reasonable adjustments to the deposition scheme. A very high concentration of MSPs above Greenland compared to lower latitudes would be required, but the opposite is the case in the standard runs. The only change to the model that successfully reproduces the observations involves PSC-based removal directly to the surface. We now discuss these results and examine a range of possible explanations for the discrepancies between the observations and modeling.

4.1. Uncertainty in the Cosmic Dust Input

The *total* cosmic dust input is estimated by Carrillo-Sánchez et al. (2016) to be $43 \pm 14 \text{ t d}^{-1}$. The uncertainty includes the stated errors in the measured Na and Fe fluxes in the upper mesosphere, and the cosmic spherule flux at the South Pole. The uncertainty in the ablated flux (which then recondenses to form MSPs) would therefore be $\pm 2.6 \text{ t d}^{-1}$. Even if this uncertainty was doubled, the upper limit to the ablation flux of 14 t d^{-1} is still well below that required to model the measured deposition fluxes in the polar regions. Furthermore, the Na and Fe fluxes that correspond to the ablation of 43 t d^{-1} are already approximately an order of magnitude larger than the injection flux required for reproducing the Na and Fe layers in WACCM (Feng et al., 2013; Marsh et al., 2013).

4.2. PSC-Based Removal of MSPs

Before discussing the results of the PSC-based removal runs, it should be noted that, as explained in section 2.3, a very simple model of PSC formation has been used to test whether this scenario is at all feasible; if so, further investigation with a more detailed model would be warranted. To obtain the agreement shown in section 3.3, PSCs have to be removed directly from the polar winter stratosphere to the surface. The validity of this scenario can be tested in several ways. First, balloon-borne aerosol number density profiles from McMurdo, Antarctica, show a minimum of $\sim 10 \text{ cm}^{-3}$ at around 16 km altitude during winter (Campbell & Deshler, 2014). A comparison of these profiles with the appropriate model run (*psc-srf-7.9*) shows that because the smaller pure sulfate aerosols are not removed significantly (since these are assumed to freeze into NAT at lower temperatures than the sulfate particles with MSP cores) there is still marginal agreement with the balloon measurements (Figure S4), although the agreement with the standard run is much better.

A second way to assess the validity of direct PSC-based removal is comparison with nitrate deposition in ice cores, as the post-nucleation growth of PSCs removes HNO_3 from the lower polar stratosphere. Although HNO_3 deposition is not tracked specifically in the model, the deposition of the mixed sulfate particle group can be used to estimate the deposition of stratospheric nitrate in the ice cores, if the sulfate:nitrate ratio in the sedimenting PSC particles is known. The minimum value of this ratio should be the equilibrium concentration of the droplets at nucleation, which gives a mass ratio of $\text{HNO}_3:\text{H}_2\text{SO}_4$ of ~ 12 (Carslaw et al., 1997). The maximum would be the difference in mass between an 80 nm radius 70 wt % H_2SO_4 droplet (the atmospheric background (Deshler et al., 2003)) and a 10 μm radius NAT particle, which results in $\text{HNO}_3:\text{H}_2\text{SO}_4 = 1.3 \times 10^6$. The difference between the sulfate fractions of the mixed sulfate deposition flux for runs *stnd-7.9* and *psc-srf-7.9* (a factor of 2–6 times higher in *psc-srf-7.9*) can then be used to estimate the sulfate deposition due to the PSC-based scheme, and multiplied by 12 to estimate a lower bound for the resulting nitrate deposition flux. Using snow accumulation rates and average nitrate concentrations at several Antarctic sites as reported by Wolff and coworkers (Wolff et al., 2010, 2012), the ice core nitrate concentrations are listed in Table 3.

The calculated nitrate deposition fluxes are a factor of 3.3–24 times higher than the observations, at the three high-latitude ice core sites. As the nitrate sources from tropospheric photochemistry have not been included in the model in this study, and as the actual nitrate/sulfate ratio may be orders of magnitude higher, this is strong evidence against the direct precipitation of PSCs to the surface in quantities large enough to account for the MSP deposition measurements. Furthermore, the pattern of the measured nitrate deposition is what would be expected from a mainly tropospheric source: the higher latitude ITASE site experiences less deposition than the lower latitude site; Law Dome on the Antarctic coast experiences the most; and EPICA on the East Antarctic plateau the least (Wolff et al., 2010, 2012). As shown in Table 3, this is the complete opposite of the pattern of calculated fluxes from the direct deposition of stratospheric PSCs.

Table 3

Comparison of Observed Nitrate Concentrations and Deposition Fluxes in Four Antarctic Ice Cores With Those Modeled by Removal as Precipitating PSCs (Lower Limit; See Text)

	Location	Calculated nitrate concentration (ng g ⁻¹)	Observed nitrate concentration (ng g ⁻¹)	Calculated nitrate flux from PSCs (g m ⁻² yr ⁻¹) × 10 ³	Observed nitrate flux ^a (g m ⁻² yr ⁻¹) × 10 ³
ITASE 02-1	82.0°S/110.0°W	114	20–25 ^b	27	4.6–5.8
ITASE 00-5	77.6°S/124.0°W	166	40–50 ^b	22	5.2–6.5
Law Dome	66.8°S/112.8°E	7.7	10–15 ^b	5.4	7.0–10.5
EPICA	75.1°S/123.2°E	242	10–50 ^c	4.8	0.2–1.0

^aCalculated from observed concentrations using snow accumulation rates. ^bFrom Wolff et al. (2012). ^cFrom Wolff et al. (2010).

Furthermore, the deposition pattern shown in Figure 1e shows that WACCM determines the average position of the Arctic polar vortex to be between the North Pole and Scandinavia, resulting in more MSP deposition in Greenland than the zonal average for that latitude. This is not an unreasonable result for the time period covered, as it has recently been shown that, between 1980 and 2009, the average position of the vortex has been moving towards Eurasia (Zhang et al., 2016). However, as the ice core measurements are historical records, the position of the polar vortex is likely to have been more evenly distributed over longitude. If this occurred in the model, the calculated deposition in Greenland would be lower, and run *psc-srf-7.9* would no longer successfully reproduce the Greenland ice core measurements.

4.3. High-Latitude Stratosphere-Troposphere Exchange

Another possible explanation for the disagreement would be if high-latitude STE was severely underestimated in both WACCM and UKCA. The resolution in the region of tropopause is about 0.5 km in UKCA and about 1.0 km in WACCM, and despite these differences, the final results are similar. Nevertheless, it is possible that some STE processes are not resolved in both models.

A significant fraction (5–40% (Liu et al., 2016)) of the tropospheric concentration of the beryllium isotopes ⁷Be and ¹⁰Be is produced in the stratosphere, and they are rapidly taken up into aerosols (Field et al., 2006), so Be isotope deposition fluxes offer another method of studying aerosols of stratospheric origin.

Liu et al. (2016) used ⁷Be specifically to investigate STE. They compared models forced by four sets of meteorological fields, one of which they believed to demonstrate excessive high-latitude STE. However, best agreement overall with observations was found using meteorological fields without high levels of local STE. Deposition observations were limited to ~20–60°N (ice core measurements are not possible due to the short half-life of ⁷Be), but surface concentration measurements were available at high latitudes. Field et al. (2006) also modeled ¹⁰Be production and transportation, and compared the results to ¹⁰Be ice core measurements at two sites in Greenland and three in Antarctica. In all cases their control run produced higher concentrations in snow than the observations, by factors of 1–6 in Greenland and 1.3–2.2 in Antarctica. A considerable percentage of this ¹⁰Be will be of stratospheric origin (5–35% (Liu et al., 2016)), and so even moderate increases in high-latitude STE would worsen the agreement.

Elsässer et al. (2015) assembled ¹⁰Be air concentration measurements and plotted them against latitude in their Figure 1; this comparison would also not benefit from a large increase in high-latitude STE. Values at high latitude are above the average by ~50% in Antarctica, and around the average in Greenland, and there is an increase from around ±65 to 70°. However, the difference in concentration is far less than would be expected if a substantial increase in STE occurred, particularly considering the low rates of precipitation at high latitudes.

The results of these studies therefore suggest that a significant increase in high-latitude STE, which would improve agreement between the models in the present study and the MSP deposition measurements, is unlikely to be valid. We have focused on Be isotopes due to their similarity to MSPs as stratospheric aerosols, but significantly increased high-latitude STE would also affect agreement with observations of other species such as O₃ (Stevenson et al., 2006).

4.4. Increased Snow Scavenging

The model of Dhomse et al. (2013) used a simplified deposition scheme based on aerosol removal under humid conditions, and where snow removed 5 times more aerosol than rain. This was because below-

cloud scavenging was assumed to be the primary deposition pathway, whereas the more advanced scheme in WACCM calculates below- and in-cloud scavenging explicitly, based on precipitation formation and fall rates. As described above, WACCM predicts in-cloud scavenging to be the dominant removal pathway, and there is no reason to expect in-cloud scavenging to be more efficient for snow than rain. This results in less deposition in Greenland, but more in Antarctica, than obtained by the simpler method of Dhomse et al. (2013).

4.5. MSP Magnetization Measurements in Ice Cores

The composition of the SP dust fraction (see section 1) was determined by analyzing the shape of the IRM acquisition curve, which indicates whether low- or high-coercivity materials are present (Lanci et al., 2012). In the case of Greenland it was concluded that 85% of the IRM was due to low-coercivity materials such as magnetite (Fe_3O_4) or maghemite ($\gamma\text{-Fe}_2\text{O}_3$), with the remainder from high-coercivity particles such as hematite ($\alpha\text{-Fe}_2\text{O}_3$) or goethite (FeOOH) (Lanci, 2004). For Vostok, Lanci et al. (2008) stated that a variable mix of high- and low-coercivity particles was present. For EPICA, there was a consistent difference between interglacial and glacial periods, where the particles had low and high coercivity, respectively.

In the calculations of MSP concentration in their subsequent study (Lanci et al., 2012), all of the MSPs are assumed to be magnetite, attributed to the high-temperature oxidation of ablating particles in the upper atmosphere. While this process is known to occur, and partially ablated micrometeorites have been observed to contain a surface magnetite layer (Love & Brownlee, 1991; Suavet et al., 2009; Toppani et al., 2001), MSPs are produced from metal atoms after they have fully ablated, and therefore, it is not clear why the Fe would then form magnetite or maghemite, when in the presence of Si- and Mg-hydroxides (Saunders & Plane, 2011). Furthermore, the Fe in MSPs should dissolve in the sulfate aerosol layer (Saunders et al., 2012), and is likely to be left as an $\text{Fe}_2(\text{SO}_4)_3$ residue before being deposited at the surface. Unfortunately, if the calculations were performed assuming a much less magnetic material, the resulting MSP concentrations and required input of cosmic dust would be much higher, resulting in an even larger discrepancy between the observations and model results of the present study.

The effects of crustal dust are taken into account by measurements of dust with radii $>0.1 \mu\text{m}$, and assuming that the ratio of small/large dust is constant. However, the shape of the dust size distribution (and the composition) is different between glacial and interglacial periods (Delmonte et al., 2004, 2002), which would produce a nonlinear correlation of measured dust concentration and SP fraction. Indeed, a weaker interglacial polar vortex was used to explain the superchondritic Ir/Pt ratio measured by Gabrielli et al. (2006) (section 1). This view is supported by dust size distribution measurements at EPICA (Delmonte et al., 2002; Delmonte et al., 2004); however, measurements at other Antarctic sites (Delmonte et al., 2004) and a recent modeling study (Kim et al., 2014) show the opposite effect. In any case, a glacial-interglacial variation in atmospheric circulation is likely, which would result in different MSP inputs during these periods. This, in addition to the size distribution variation mentioned above, indicates that treating the glacial and interglacial values separately is probably preferable when comparing to present-day models.

If only interglacial data points from the magnetization measurements are included (~ 26 points), the SP intercept for Vostok (proportional to MSP input) would be $(65 \pm 46)\%$ of the original value. For NGRIP there would be no correlation between SP and dust concentration (but only eight data points). This is also the case for EPICA (~ 17 points), although it does not exhibit the same relationship between dust concentrations and glacial/interglacial periods. Including only low-dust results would similarly give no correlation.

Carrillo-Sánchez et al. (2016) recently determined that $\sim 82\%$ of the incoming cosmic dust is unablated, and more than 99% of the mass of unablated particles is contained in particles with $r > 3.8 \mu\text{m}$. These are too large to be single-domain (SD) magnetite particles, but multidomain (MD) grains which could contain some magnetite that might contribute to the SP signal (Lanci et al., 2007). However, the magnetization of these MD particles would be around an order of magnitude smaller than the single-domain particles (L. Lanci, Università di Urbino, personal communications). Particles of this size would be measured by the Coulter counters, but would be in concentrations of $\sim 0.13 \text{ ng g}^{-1}$ in Greenland and $\sim 1.5 \text{ ng g}^{-1}$ in Antarctica, which compares to total dust concentrations that are much higher, within the range of 4–8000 ng g^{-1} . Hence, any SP magnetization they caused would add to the intercept of SP versus total dust concentration plots (see section 1). This would contribute no more than 45% of the magnetization due to SD magnetite MSPs, assuming 18%

of cosmic dust ablates, all unablated dust is made up of MD magnetite (with 10% of the magnetization of SD magnetite), and unablated material is deposited uniformly across the globe. That is, micrometeorites should make a limited contribution to the SP measurements, reducing the required cosmic dust input by a factor of less than 1.45, which is not enough to achieve agreement with the observations. Furthermore, the number flux of these micrometeorites is too small for them to occur regularly enough in ice core samples to produce a reasonably statistical contribution to the SP measurements (unless substantial fragmentation of cosmic dust during atmospheric entry occurs).

A further point is that micrometeorites are likely to be composed mostly of iron-rich olivines or pyroxenes (see section 1), which would not produce the observed magnetization. It is possible that the olivine could be converted to magnetite through the process of serpentinization in the ice. The rate at which this occurs in *liquid* H₂O at 298 K and a pH of 5.2 (typical of an ice core) is $6.5 \times 10^{-14} \text{ mol cm}^{-2} \text{ s}^{-1}$ (Wogelius & Walther, 1992). Extrapolating to an ice core temperature of 260 K using an activation energy of 70 kJ mol^{-1} (Lasaga et al., 1994), the rate decreases to $1.0 \times 10^{-15} \text{ mol cm}^{-2} \text{ s}^{-1}$. The olivine in a $50 \text{ }\mu\text{m}$ radius micrometeorite would then be converted to magnetite in about 700 years, which is an appropriate time scale. However, the serpentinization rate does not appear to have been measured in ice as opposed to liquid H₂O, and is probably significantly slower.

Lastly, the modeled size distribution of the deposited MSPs at the deposition sites is presented in Figure S5, which shows that for the standard run (*std-7.9*), most of the MSP mass is predicted to be in particles larger than the $\sim 10 \text{ nm}$ radius limit for contribution to the SP signal (Lanci et al., 2012). For run *sep-7.9*, only 0.2% of the particles were below this size. In fact, it is likely that CARMA underestimates the MSP coagulation rates, which should be enhanced by the long-range magnetic dipole interactions of the Fe-rich particles (Saunders & Plane, 2010), which is not yet included in CARMA.

4.6. Pt/Ir Measurements in Ice Cores

Gabrielli and coworkers estimated the cosmic dust input by measuring Ir and Pt concentrations in ice, after dissolution in nitric acid (Gabrielli et al., 2004, 2006). This process was expected to only dissolve Ir and Pt from MSP particles ($r < 100 \text{ nm}$). For larger micrometeorites ($> 3 \text{ }\mu\text{m}$), probably less than 10% of the total Ir and Pt would dissolve (P. Gabrielli, Ohio State University, personal communications). However, this relates to spherical particles, whereas MSPs are likely to be fractal-like and porous (Saunders & Plane, 2006), with a greater surface area available for dissolution. As an upper limit, if 100% of the Ir and Pt dissolved, an MSP deposition flux of $15.4 \times 10^{-5} \text{ g m}^{-2} \text{ yr}^{-1}$ would include the 35.4 t d^{-1} unablated fraction and the results from model run *unab-43* would apply. This would reduce the observed/calculated ratio to 3.3–5.7 and 0.37–1.6 for Greenland and Antarctica, respectively. However, this comparatively good agreement assumes complete dissolution of Ir and Pt in micrometeorites, and also ignores the fact that this would produce a much more stochastic pattern to the measured MSP deposition flux, as pointed out by Gabrielli et al. (2004).

Another point to consider is that the measured Ir/Pt ratio in Greenland during the Holocene is, on average, close to the chondritic ratio of 0.49 (Gabrielli et al., 2004). This is surprising given recent advances in understanding differential ablation (Gómez Martín et al., 2017). Carrillo-Sánchez et al. (2016) predicted elemental ablation fractions of 21% for Fe, 17% for Si, 10% for Ca, and 7% for Al. Although the elements Ir and Pt are not included in the Chemical Ablation Model (CABMOD) (Vondrak et al., 2008) used in that study, the vapor pressures of these elements above their pure liquid phases lie between those of Fe and Ca above a silicate melt (Figure S6). This indicates that 10–21% of these elements should ablate, with Pt ablating more readily than Ir. This has two implications: first, that the Ir/Pt ratio should be less than 0.49 in MSPs; and second, that using the Ir and Pt fluxes as markers of the cosmic dust input implies that the total input is a factor of 5–10 times larger than the already very large $214 \pm 82 \text{ t d}^{-1}$ estimated by Gabrielli et al. (2004).

It is therefore worth considering contamination of the ice cores by other sources of Ir and Pt. Gabrielli et al. (2006) concluded that continuous quiescent volcanic degassing (most likely from Mount Erebus) contributed to increased levels of Ir (Koeberl, 1989) during interglacial periods in Antarctica. In the Greenland study (Gabrielli et al., 2004), volcanic eruptions were ruled out due to Ir species reacting rapidly with available particulates and being deposited close to the source. However, the Icelandic volcanoes are a similar distance from GRIP as Mount Erebus is from EPICA, and Gabrielli et al. (2008) later found evidence of transport of

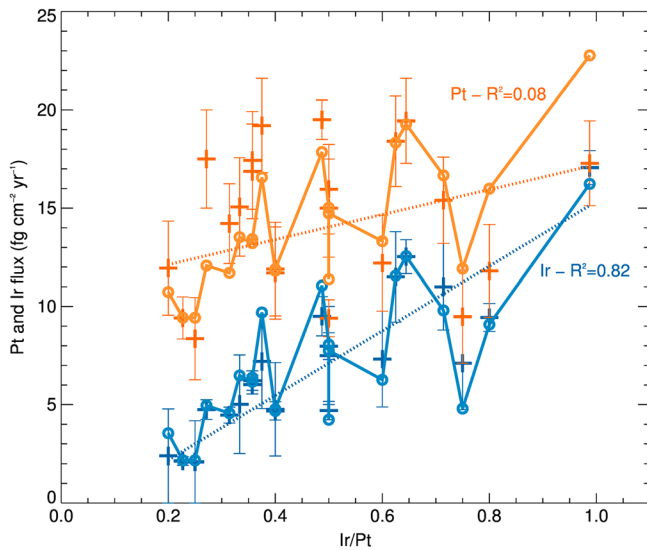


Figure 2. Correlation between the Ir (blue) and Pt (orange) fluxes and the Ir/Pt ratio for the Holocene from GRIP (Gabielli et al., 2004), assuming a volcanic source in addition to MSPs. The crosses show measured values in the ice core, and the circles and lines show the fit of a simple linear combination of sources (see text). The dotted lines show the linear fits to which the R^2 values refer. The positive correlation between Φ_{Ir} and Ir/Pt, and absence of a negative correlation between Φ_{Pt} and Ir/Pt, indicates an additional source with a greater Ir/Pt ratio than in MSPs.

volcanic fallout from Iceland to GRIP. The ice core sections analyzed from GRIP have a time resolution of 2 to 10 years; therefore, some or all of the GRIP Ir measurements could include a contribution from regularly erupting Icelandic volcanoes (Thordarson & Larsen, 2007). A similar case can be made for Pt. In 2004, it was not known whether Pt was enriched in volcanic emissions (Gabielli et al., 2004); however, this has now been shown to be the case (Soyol-Erdene et al., 2011; Yudovskaya et al., 2008). In fact, increases in Pt deposition seen in Greenland were attributed to recent volcanic emissions (Gabielli et al., 2008), and superchondritic Ir/Pt ratios from the Antarctica study coincided with an increase in the Pt flux (Gabielli et al., 2006).

Although the average Ir/Pt ratio in the Holocene measurements at GRIP was 0.49 (close to the chondritic (CI) ratio), the ratio for individual data points varied between 0.20 and 0.99 (Gabielli et al., 2004). Also, all but two of the data points during the preceding glacial period were in this range with an average of 0.55 (excluding two very high Ir/Pt ratios of 2.50 and 2.91). Figure 2 is a correlation plot between the deposition fluxes of Ir and Pt and the Ir/Pt ratio (the measured values are depicted as crosses, and the dotted lines and R^2 values are from a simple linear fit to indicate the strength of the correlations). The positive correlation between the Ir flux and Ir/Pt, but absence of a correlation for the measured Pt, is evidence for a superchondritic Ir source (most likely volcanic), in addition to a constant MSP source with a low Ir/Pt ratio because Ir is more refractory (see above).

The Ir flux can then be expressed as

$$\Phi_i^{Ir} = \alpha^{Ir} \Phi_{MSP} + c_i \beta^{Ir} \Phi_V \tag{3}$$

where Φ_i^{Ir} is the Ir flux for data point i in the ice core record; α^{Ir} is the fraction of Ir in the MSPs; Φ_{MSP} is the MSP flux, assumed constant; and c_i is a coefficient (≥ 0) for the contribution of a non-MSP source flux Φ_V , with a relative Ir abundance β^{Ir} . There is an analogous equation for the Pt flux. As discussed above, between 10% and 21% of Ir and Pt is likely to ablate, with Pt more volatile than Ir. The chondritic ratio is Ir/Pt = 0.49; therefore, the minimum possible Ir/Pt ratio in MSPs would be $10/21 \times 0.49 = 0.23$. This was used in the fit as the fixed value for α^{Ir}/α^{Pt} , with Φ_{MSP} fixed to give the absolute Ir flux at this value (Figure 2). The ratio β^{Ir}/β^{Pt} and Φ_V were then optimized in a global fit to the data points. The relative contribution of the non-MSP source in each ice core sample, c_i , was allowed to float for each data point as this would not be constant with time. Note that the problem is overdetermined because there are $2N$ equations if there are N samples, but the number of unknowns is $N + 2$. As shown in Figure 2, a reasonably good fit to the measured points can be obtained, yielding $\beta^{Ir}/\beta^{Pt} = 1.05$ and MSP Ir and Pt fluxes of 2.2 ± 0.2 and $9.4 \pm 0.8 \text{ fg cm}^{-2} \text{ yr}^{-1}$, respectively, where the uncertainty is the 1σ standard deviation of the fit parameter. Using the same MSP Ir/Pt ratio of 0.23, the total MSP flux is equal to $(8.3 \pm 0.7) \times 10^{-5} \text{ g m}^{-2} \text{ yr}^{-1}$, a factor of 1.9 less than the original results (Gabielli et al., 2004).

A similar correlation of Ir and Pt against Ir/Pt is found for the LGA data points from EPICA (Figure S7), and an equivalent fit results in an MSP flux of $(1.8 \pm 0.4) \times 10^{-5} \text{ g m}^{-2} \text{ yr}^{-1}$, a factor of 2.6 less than the original results (Gabielli et al., 2006). The fitted β^{Ir}/β^{Pt} is 1.08 for EPICA, which is very close to the value for GRIP. The revised values for the GRIP and EPICA fluxes are listed in Table 2, and are in much better agreement with the fluxes derived from the superparamagnetic Fe measurements in Table 3. No correlation for either element was found for Vostok (Figure S7), so that the Vostok data cannot be used for analogous fits.

4.7. Nanodust From the Inner Solar System

Small interplanetary dust particles ($r < 1 \mu\text{m}$) tend to be blown out of the solar system by radiation pressure, rather than their orbits being circularized by Poynting-Robertson drag (Dermott et al., 2001; Nesvorný et al., 2010). Nevertheless, fine dust of $r \sim 10 \text{ nm}$ should be produced from comets while in the inner solar system, and therefore contribute some of the cosmic dust flux at Earth (Czechowski & Mann, 2010; Le Chat et al.,

2013; Schippers et al., 2014). However, 99% of the total mass flux would still be within particles larger than about 3 μm , using the cumulative flux in Figure 3 of Schippers et al. (2014).

4.8. Meteoroid Fragmentation

If incoming cosmic dust particles experience pressures higher than their tensile strength during atmospheric entry, then they can undergo fragmentation. This process has been observed for some large particles by meteor luminosity measurements (Blum et al., 2014, 2015). Hornung et al. (2016) recently reported the collection of cometary dust particles at low-impact velocities using the COSIMA instrument on the ROSETTA spacecraft, from which they deduced the pressure required for fragmentation (i.e., the tensile strength) to be between ~ 0.8 and 14 kPa. Other modeling and observational studies of cometary material tensile strengths on the 10–100 μm scale are in agreement with these values (Bar-Nun et al., 2007; Biele et al., 2009).

The CABMOD model (Vondrak et al., 2008) can be used to estimate the maximum pressure exerted on a meteoroid of specified mass by collision with air molecules before it melts, for a range of entry zenith angles and velocities. The pressure is calculated as the kinetic energy density, $\sigma_{ed} = \frac{1}{2}\rho v^2$, where ρ is the atmospheric density and v is the meteoroid velocity. Figure S9 shows an example of the maximum pressure as a function of initial particle size and velocity, for one entry angle (others are very similar). Taking into account the size and velocity distributions from Carrillo-Sánchez et al. (2016), 95% of particles (by mass) will experience pressures of only 35–400 Pa. Hence, based on the tensile strengths discussed above, fragmentation should not produce a significant flux of sub-micron particles carrying Ir and Pt to the surface.

However, another possibility is that fragmentation could occur during atmospheric entry if, before the main silicate phases melt, the “glue” cementing the mineral grains in the meteoroid evaporates, for example, if it were an organic substance or a Na-rich mineral. This process has been suggested by Subasinghe et al. (2016) to account for their observations with high-resolution cameras of meteor light curves. They report that $>90\%$ of meteors that they have observed fragment to some extent. Only millimeter-sized meteoroids can be observed by this method, but the same process may cause fragmentation of smaller meteoroids if they became sufficiently hot during atmospheric entry. Depending on the size of the fragments, this process could result in material small enough to be transported with the atmospheric circulation (if there are significant small fragments with $r < 100$ nm), rather than only sedimenting rapidly across the tropopause. Like MSPs, smaller fragments ($r < 0.5$ μm) would build up in the lower stratosphere. Aircraft-based measurements of stratospheric sulfate aerosol found that Fe-containing particles were composed of 0.5–1.0% meteoric Fe by mass (Cziczo et al., 2001). Using the same size limits as the measurements and averaged over the same spatial range, the standard *stnd-7.9* model run predicts this value to be 0.3–0.4%. Therefore, there is scope for the presence of more stratospheric Fe, by up to about a factor of 3. A final point is that a large number of smaller fragments would make the counting statistics in the ice core sections much less stochastic compared with unfragmented micrometeorites.

4.9. Changes in the Cosmic Dust Flux Over Time

It is of course possible that the cosmic dust input rate has decreased over the course of the Holocene. The GRIP ice core measurements range from ~ 700 to 11,500 years before present (Gabielli et al., 2004), and the useable MSP measurements in Antarctica from $\sim 18,000$ to 217,000 years before present (Gabielli et al., 2006). In contrast, the Fe and Na atom vertical flux measurements (Gardner et al., 2014; Huang et al., 2015) used by Carrillo-Sánchez et al. (2016) to constrain the cosmic dust mass input rate are contemporary. An approximately 100 kyr periodicity in the cosmic dust flux was suggested by Farley and Patterson (1995) and Patterson and Farley (1998) based on ^3He measurements. However, this has more recently been attributed to varying focusing of sediments by ocean currents (Higgins et al., 2002; Marcantonio et al., 1999; Winckler et al., 2004), and a constant flux of extraterrestrial ^3He has been found in Antarctic ice cores (Winckler & Fischer, 2006). In addition to this periodicity, sharp spikes in the ^3He record have been occasionally observed, possibly attributable to the close passage of a single comet or major asteroidal collision event (Patterson & Farley, 1998). More specifically, it has been suggested that a large fraction of the recent cosmic dust input is due to the disintegration of a single body (Comet Encke), and this input has steadily decreased over a time scale of ~ 10 kyr (Steel et al., 1991). Therefore, a significant decrease during the Holocene is

possible, but there is no clear evidence to support this and it would need to have occurred within the last millennium.

5. Summary and Conclusions

Ice core observations of MSPs from superparamagnetic Fe and Ir/Pt measurements, in both Greenland and Antarctica, show much higher deposition fluxes than predicted by the WACCM chemistry-climate model with CARMA aerosol microphysics, using an MSP input of 7.9 t d^{-1} which is consistent with the vertical fluxes of Na and Fe atoms in the upper mesosphere (Carrillo-Sánchez et al., 2016). The observed/modeled ratios are 33–56 in Greenland and 11–36 in Antarctica. The low deposition fluxes predicted at the ice core locations arise because of a lack of enhancement of MSP deposition at high latitudes: the deposition enhancement ratios are 0.49 and 0.21 for Greenland and Antarctica, respectively. The required input to match observations in Greenland and Antarctica, assuming that deposition rates scale linearly with the input, would be 250 and 95 t d^{-1} , respectively. These are within the upper limit of previous literature values (Plane, 2012), but much greater than the most recently value which is constrained by multiple observations (Carrillo-Sánchez et al., 2016).

After inspection of the Ir/Pt measurements, there is evidence for another source with a higher Ir/Pt ratio than MSPs, at least in the GRIP (Holocene) and EPICA (Last Glacial Age) data. This source is likely to be volcanic, as both sites have been shown to be subject to volcanic fallout, and Pt and Ir are both enriched in volcanic emissions with respect to their crustal composition. Reanalysis of this data results in decreased flux values with observed/modeled ratios of 30–33 in Greenland and 11–13 in Antarctica.

Changes to the deposition scheme in the model were explored: below-cloud scavenging was parameterized based on aerosol size, and dry deposition increased to reduce the washout of MSPs at midlatitudes. However, neither of these options resulted in a significant change to the pattern of MSP deposition. A further run was performed using the UKCA model, which has much finer vertical resolution around the tropopause, but this shows general agreement with WACCM, and even lower deposition enhancement ratios in Greenland. A significant increase in STE at high latitudes would improve agreement, but Be isotope studies suggest that this is unlikely.

If MSP-nucleated PSCs sediment directly from the polar winter stratosphere to the surface, then satisfactory agreement between the modeled and measured MSP deposition rate can be achieved. However, while the measured aerosol concentrations in the lower stratosphere and extinction/backscatter measurements do not completely rule out such a process, the excessive nitrate deposition that would result makes this extremely unlikely. The approach of allowing the sedimenting PSCs to evaporate in the troposphere before reaching the surface produces only a limited improvement in agreement of the model with the MSP deposition measurements. A simple PSC scheme was used here, which could be improved with a full treatment of heterogeneous nucleation and particle growth, although it is difficult to see how this would reduce the discrepancy with the measurements.

Since only ~18% of the incoming cosmic dust mass ablates, there is another 35 t d^{-1} of unablated material which enters the atmosphere (Carrillo-Sánchez et al., 2016). If much of this dust fragments during atmospheric entry into sub-micron particles (which are too small to ablate), then the observed/modeled ratios would be reduced to values of 3.1–3.3 and 0.5–0.6 in Greenland and Antarctica, respectively. However, while these values represent much better agreement, there is no direct evidence for fragmentation of meteoroids smaller than $100 \mu\text{m}$ in radius.

In conclusion, it appears that none of the explanations considered here can fully account for the marked disagreement between the measured and modeled MSP deposition fluxes. This is the case both for the absolute and the relative fluxes in Greenland and Antarctica. There are a number of directions for future research that may help to resolve these discrepancies. First, the ablated meteoric flux—for example, the MSP source—is tied to the fluxes of Na and Fe atoms measured by lidar in the upper mesosphere (Carrillo-Sánchez et al., 2016). However, these measurements have only been made in a handful of locations by the groups of Gardner (Gardner et al., 2014, 2016) and Chu (Huang et al., 2015). More measurements over a range of latitudes would be very desirable. Second, the contribution of volcanic sources of Ir and Pt to the MSP signal in ice cores needs to be better understood, as well as the potential contribution of larger meteoric

fragments to the Ir and Pt signals. Third, the separation of the glacial and interglacial data in Fe superparamagnetic observations, and a better understanding of how highly magnetized sub-100 nm particles are produced in the atmosphere, is needed. Fourth, the model predicts relatively high MSP deposition rates over the Himalayas and Canadian Rockies (Figure 1), which suggests that glacial ice core measurements in these locations should be a priority.

Acknowledgments

This work was supported by the European Research Council (project 291332–CODITA). The MERRA-2 data sets used in this study were provided by the Global Modeling and Assimilation Office (GMAO) at NASA Goddard Space Flight Center. The WACCM data sets generated for this work have been archived at the Leeds University PetaByte Environmental Tape Archive and Library (PETAL; <http://www.see.leeds.ac.uk/business-and-consultation/facilities/petabyte-environmental-tape-archive-and-library-petal/>). The data and fits described in section 19, and the MOZART preprocessor input file, are included in the supporting information.

References

- Andersen, K. K., Azuma, N., Barnola, J.-M., Bigler, M., Biscaye, P., Caillon, N., ... North Greenland Ice Core Project members, North Greenland Ice Core Project members (2004). High-resolution record of Northern Hemisphere climate extending into the last interglacial period. *Nature*, *431*, 147–151.
- Asplund, M., Grevesse, N., Sauval, A. J., & Scott, P. (2009). The Chemical Composition of the Sun. In R. Blandford, J. Kormendy, & E. van Dishoeck (Eds.), *Ann. Rev. Astron. Astrophys* (pp. 481–522). Palo Alto: Annual Reviews. <https://doi.org/10.1146/annurev.astro.46.060407.145222>
- Augustin, L., Barbante, C., Barnes, P. R. F., Barnola, J. M., Bigler, M., Castellano, E., ... EPICA Community Members, EPICA Community Members (2004). Eight glacial cycles from an Antarctic ice core. *Nature*, *429*, 623–628.
- Bardeen, C. G., Toon, O. B., Jensen, E. J., Marsh, D. R., & Harvey, V. L. (2008). Numerical simulations of the three-dimensional distribution of meteoric dust in the mesosphere and upper stratosphere. *Journal of Geophysical Research*, *113*, D17202. <https://doi.org/10.1029/2007JD009515>
- Barker, J. L., & Anders, E. (1968). Accretion rate of cosmic matter from iridium and osmium contents of deep-sea sediments. *Geochimica et Cosmochimica Acta*, *32*, 627–645.
- Bar-Nun, A., Pat-El, I., & Laufer, D. (2007). Comparison between the findings of Deep Impact and our experimental results on large samples of gas-laden amorphous ice. *Icarus*, *187*, 321–325.
- Biele, J., Ulamec, S., Richter, L., Knollenberg, J., Kuehrt, E., & Moehlmann, D. (2009). The putative mechanical strength of comet surface material applied to landing on a comet. *Acta Astronautica*, *65*, 1168–1178.
- Blum, J., Gundlach, B., Muehle, S., & Trigo-Rodriguez, J. M. (2014). Comets formed in solar-nebula instabilities!—An experimental and modeling attempt to relate the activity of comets to their formation process. *Icarus*, *235*, 156–169.
- Blum, J., Gundlach, B., Muehle, S., & Trigo-Rodriguez, J. M. (2015). Comets formed in solar-nebula instabilities—An experimental and modeling attempt to relate the activity of comets to their formation process. *Icarus*, *248*, 135–136.
- Brook, E. J., Kurz, M. D., Curtice, J., & Cowburn, S. (2000). Accretion of interplanetary dust in polar ice. *Geophysical Research Letters*, *27*, 3145–3148.
- Campbell, P., & Deshler, T. (2014). Condensation nuclei measurements in the midlatitude (1982–2012) and Antarctic (1986–2010) stratosphere between 20 and 35 km. *Journal of Geophysical Research: Atmospheres*, *119*, 137–152. <https://doi.org/10.1002/2013JD019710>
- Carrillo-Sánchez, J. D., Nesvorný, D., Pokorný, P., Janches, D., & Plane, J. M. C. (2016). Sources of cosmic dust in the Earth's atmosphere. *Geophysical Research Letters*, *43*, 11,979–911,986. <https://doi.org/10.1002/2016GL071697>
- Carrillo-Sánchez, J. D., Plane, J. M. C., Feng, W., Nesvorný, D., & Janches, D. (2015). On the size and velocity distribution of cosmic dust particles entering the atmosphere. *Geophysical Research Letters*, *42*, 6518–6525. <https://doi.org/10.1002/2015GL065149>
- Carslaw, K. S., Kettleborough, J. A., Northway, M. J., Davies, S., Gao, R. S., Fahey, D. W., ... Kleinbohl, A. (2002). A vortex-scale simulation of the growth and sedimentation of large nitric acid hydrate particles. *Journal of Geophysical Research*, *107*(D20), 8300. <https://doi.org/10.1029/2001JD000467>
- Carslaw, K. S., Peter, T., & Clegg, S. L. (1997). Modeling the composition of liquid stratospheric aerosols. *Reviews of Geophysics*, *35*, 125–154.
- Czechowski, A., & Mann, I. (2010). Formation and acceleration of nano dust in the inner heliosphere. *The Astrophysical Journal*, *714*, 89–99.
- Cziczo, D. J., Thomson, D. S., & Murphy, D. M. (2001). Ablation, flux, and atmospheric implications of meteors inferred from stratospheric aerosol. *Science*, *291*, 1772–1775.
- Dansgaard, W., Johnsen, S. J., Clausen, H. B., Dahljensen, D., Gundestrup, N. S., Hammer, C. U., ... Bond, G. (1993). Evidence for general instability of past climate from a 250-kyr ice-core record. *Nature*, *364*, 218–220.
- Delmonte, B., Petit, J. R., Andersen, K. K., Basile-Doelsch, I., Maggi, V., & Ya Lipenkov, V. (2004). Dust size evidence for opposite regional atmospheric circulation changes over east Antarctica during the last climatic transition. *Climate Dynamics*, *23*.
- Delmonte, B., Petit, J., & Maggi, V. (2002). Glacial to Holocene implications of the new 27,000-year dust record from the EPICA Dome C (East Antarctica) ice core. *Climate Dynamics*, *18*, 647–660.
- Dermott, S. F., Kehoe, T. J. J., Grogan, K., Durda, D. D., Jayaraman, S., Kortenkamp, S. J., & Wyatt, M. C. (2001). Orbital Evolution of Interplanetary Dust. In E. Grün, B. Å. S. Gustafson, S. Dermott, & H. Fechtig (Eds.), *Interplanetary Dust* (pp. 569–639). Berlin, Heidelberg: Springer Berlin Heidelberg. https://doi.org/10.1007/978-3-642-56428-4_12
- Deshler, T., Hervig, M. E., Hofmann, D. J., Rosen, J. M., & Liley, J. B. (2003). Thirty years of in situ stratospheric aerosol size distribution measurements from Laramie, Wyoming (41°N), using balloon-borne instruments. *Journal of Geophysical Research*, *108*(D5), 4167. <https://doi.org/10.1029/2002JD002514>
- Dhomse, S. S., Emmerson, K. M., Mann, G. W., Bellouin, N., Carslaw, K. S., Chipperfield, M. P., ... Thomason, L. W. (2014). Aerosol microphysics simulations of the Mt. Pinatubo eruption with the UM-UKCA composition-climate model. *Atmospheric Chemistry and Physics*, *14*, 11,221–11,246.
- Dhomse, S. S., Saunders, R. W., Tian, W., Chipperfield, M. P., & Plane, J. M. C. (2013). Plutonium-238 observations as a test of modeled transport and surface deposition of meteoric smoke particles. *Geophysical Research Letters*, *40*, 4454–4458. <https://doi.org/10.1002/grl.50840>
- Elsässer, C., Wagenbach, D., Levin, I., Stanzick, A., Christl, M., Wallner, A., ... Dibb, J. (2015). Simulating ice core 10-Be on the glacial–interglacial timescale. *Climate of the Past*, *11*, 115–133.
- English, J. M., Toon, O. B., & Mills, M. J. (2012). Microphysical simulations of sulfur burdens from stratospheric sulfur geoengineering. *Atmospheric Chemistry and Physics*, *12*, 4775–4793.
- English, J. M., Toon, O. B., Mills, M. J., & Yu, F. (2011). Microphysical simulations of new particle formation in the upper troposphere and lower stratosphere. *Atmospheric Chemistry and Physics*, *11*, 9303–9322.
- Esser, B. K., & Turekian, K. K. (1993). The osmium isotopic composition of the continental crust. *Geochimica et Cosmochimica Acta*, *57*, 3093–3104.

- Fahey, D. W., Gao, R. S., Carslaw, K. S., Kettleborough, J., Popp, P. J., Northway, M. J., ... von König, M. (2001). The detection of large HNO_3 -containing particles in the winter arctic stratosphere. *Science*, *291*, 1026–1031.
- Farley, K. A., & Patterson, D. B. (1995). A 100-kyr periodicity in the flux of extraterrestrial ^3He to the sea-floor. *Nature*, *378*, 600–603.
- Feierabend, K. J., Havey, D. K., Brown, S. S., & Vaida, V. (2006). Experimental absolute intensities of the $4\nu_9$ and $5\nu_9$ O–H stretching overtones of H_2SO_4 . *Chemical Physics Letters*, *420*, 438–442.
- Feng, W., Marsh, D. R., Chipperfield, M. P., Janches, D., Höffner, J., Yi, F., & Plane, J. M. C. (2013). A global atmospheric model of meteoric iron. *Journal of Geophysical Research: Atmospheres*, *118*, 9456–9474. <https://doi.org/10.1002/jgrd.50708>
- Field, C. V., Schmidt, G. A., Koch, D., & Salyk, C. (2006). Modeling production and climate-related impacts on ^{10}Be concentration in ice cores. *Journal of Geophysical Research*, *111*, D15107. <https://doi.org/10.1029/2005JD006410>
- Fueglistaler, S., Luo, B. P., Buss, S., Wernli, H., Voigt, C., Müller, M., ... Peter, T. (2002). Large NAT particle formation by mother clouds: Analysis of SOLVE/THESEO-2000 observations. *Geophysical Research Letters*, *29*(12), 1610. <https://doi.org/10.1029/2001GL014548>
- Gabrielli, P., Barbante, C., Plane, J. M. C., Boutron, C. F., Jaffrezo, J. L., Mather, T. A., ... Cescon, P. (2008). Siderophile metal fallout to Greenland from the 1991 winter eruption of Hekla (Iceland) and during the global atmospheric perturbation of Pinatubo. *Chemical Geology*, *255*, 78–86.
- Gabrielli, P., Barbante, C., Plane, J. M. C., Varga, A., Hong, S., Cozzi, G., ... Boutron, C. F. (2004). Meteoric smoke fallout over the Holocene epoch revealed by iridium and platinum in Greenland ice. *Nature*, *432*, 1011–1014.
- Gabrielli, P., Plane, J. M. C., Boutron, C. F., Hong, S., Cozzi, G., Cescon, P., ... Barbante, C. (2006). A climatic control on the accretion of meteoric and super-chondritic iridium–platinum to the Antarctic ice cap. *Earth and Planetary Science Letters*, *250*, 459–469.
- Ganapathy, R., Brownlee, D. E., & Hodge, P. W. (1978). Silicate spherules from deep-sea sediments—Confirmation of extraterrestrial origin. *Science*, *201*, 1119–1121.
- Gardner, C. S., Liu, A. Z., & Guo, Y. (2016). Vertical and horizontal transport of mesospheric Na: Implications for the mass influx of cosmic dust. *Journal of Atmospheric and Solar-Terrestrial Physics*. <https://doi.org/10.1016/j.jastp.2016.1007.1013>
- Gardner, C. S., Liu, A. Z., Marsh, D. R., Feng, W., & Plane, J. M. C. (2014). Inferring the global cosmic dust influx to the Earth's atmosphere from lidar observations of the vertical flux of mesospheric Na. *Journal of Geophysical Research: Space Physics*, *119*, 7870–7879. <https://doi.org/10.1002/2014JA020383>
- Gómez Martín, J. C., Bones, D. L., Carrillo-Sánchez, J. D., James, A. D., Trigo-Rodríguez, J. M., Fegley, B. Jr., & Plane, J. M. C. (2017). Novel experimental simulations of the atmospheric injection of meteoric metals. *The Astrophysical Journal*, *836*, 212.
- Hervig, M. E., Deaver, L. E., Bardeen, C. G., Russell, J. M. III, Bailey, S. M., & Gordley, L. L. (2012). The content and composition of meteoric smoke in mesospheric ice particles from SOFIE observations. *Journal of Atmospheric and Solar-Terrestrial Physics*, *84–85*, 1–6.
- Higgins, S. M., Anderson, R. F., Marcantonio, F., Schlosser, P., & Stute, M. (2002). Sediment focusing creates 100-ka cycles in interplanetary dust accumulation on the Ontong Java Plateau. *Earth and Planetary Science Letters*, *203*, 383–397.
- Hornung, K., Merouane, S., Hilchenbach, M., Langevin, Y., Mellado, E. M., Della Corte, V., ... Cosima Team, Cosima Team (2016). A first assessment of the strength of cometary particles collected in-situ by the COSIMA instrument onboard ROSETTA. *Planetary and Space Science*, *133*, 63–75.
- Hoyle, C. R., Engel, I., Luo, B. P., Pitts, M. C., Poole, L. R., Grooss, J. U., & Peter, T. (2013). Heterogeneous formation of polar stratospheric clouds—Part 1: Nucleation of nitric acid trihydrate (NAT). *Atmospheric Chemistry and Physics*, *13*, 9577–9595.
- Huang, W., Chu, X., Gardner, C. S., Carrillo-Sánchez, J. D., Feng, W., Plane, J. M. C., & Nesvorný, D. (2015). Measurements of the vertical fluxes of atomic Fe and Na at the mesopause: Implications for the velocity of cosmic dust entering the atmosphere. *Geophysical Research Letters*, *42*, 169–175. <https://doi.org/10.1002/2014GL062390>
- Hughes, D. W. (1978). Meteors. In J. A. M. McDonnell (Ed.), *Cosmic Dust* (pp. 123–185). London: Wiley.
- Hurrell, J. W., Holland, M. M., Gent, P. R., Ghan, S., Kay, J. E., Kushner, P. J., ... Marshall, S. (2013). The Community Earth System Model: A framework for collaborative research. *Bulletin of the American Meteorological Society*, *94*, 1339–1360.
- Kalashnikova, O., Horanyi, M., Thomas, G. E., & Toon, O. B. (2000). Meteoric smoke production in the atmosphere. *Geophysical Research Letters*, *27*, 3293–3296.
- Karner, D. B., Levine, J., Müller, R. A., Asaro, F., Ram, M., & Stolz, M. R. (2003). Extraterrestrial accretion from the GISP2 ice core. *Geochimica et Cosmochimica Acta*, *67*, 751–763.
- Kim, S.-J., Lü, J., & Kim, B.-M. (2014). The Southern Annular Mode (SAM) in PMIP2 simulations of the last glacial maximum. *Advances in Atmospheric Sciences*, *31*, 863–878.
- Kinnison, D. E., Brasseur, G. P., Walters, S., Garcia, R. R., Marsh, D. R., Sassi, F., ... Simmons, A. J. (2007). Sensitivity of chemical tracers to meteorological parameters in the MOZART-3 chemical transport model. *Journal of Geophysical Research*, *112*, D20302. <https://doi.org/10.1029/2006JD007879>
- Koeberl, C. (1989). Iridium enrichment in volcanic dust from blue ice fields, Antarctica, and possible relevance to the K/T boundary event. *Earth and Planetary Science Letters*, *92*, 317–322.
- Kyte, F. T., & Wasson, J. T. (1986). Accretion rate of extraterrestrial matter—Iridium deposited 33 to 67 million years ago. *Science*, *232*, 1225–1229.
- Lamarque, J. F., Emmons, L. K., Hess, P. G., Kinnison, D. E., Tilmes, S., Vitt, F., ... Tyndall, G. K. (2012). CAM-Chem: Description and evaluation of interactive atmospheric chemistry in the Community Earth System Model. *Geoscientific Model Development*, *5*, 369–411.
- Lanci, L. (2004). Magnetization of Greenland ice and its relationship with dust content. *Journal of Geophysical Research*, *109*, D09104. <https://doi.org/10.1029/2003JD004433>
- Lanci, L., Delmonte, B., Kent, D. V., Maggi, V., Biscaye, P. E., & Petit, J. R. (2012). Magnetization of polar ice: a measurement of terrestrial dust and extraterrestrial fallout. *Quaternary Science Reviews*, *33*, 20–31.
- Lanci, L., Delmonte, B., Maggi, V., Petit, J. R., & Kent, D. V. (2008). Ice magnetization in the EPICA-Dome C ice core: Implication for dust sources during glacial and interglacial periods. *Journal of Geophysical Research*, *113*, D14207. <https://doi.org/10.1029/2007JD009678>
- Lanci, L., & Kent, D. V. (2006). Meteoric smoke fallout revealed by superparamagnetism in Greenland ice. *Geophysical Research Letters*, *33*, L13308. <https://doi.org/10.1029/2006GL026480>
- Lanci, L., Kent, D. V., & Biscaye, P. E. (2007). Meteoric smoke concentration in the Vostok ice core estimated from superparamagnetic relaxation and some consequences for estimates of Earth accretion rate. *Geophysical Research Letters*, *34*, L10803. <https://doi.org/10.1029/2007GL029811>
- Lane, J. R., & Kjaergaard, H. G. (2008). Calculated electronic transitions in sulfuric acid and implications for its photodissociation in the atmosphere. *The Journal of Physical Chemistry. A*, *112*, 4958–4964.
- Lasaga, A. C., Soler, J. M., Ganor, J., Burch, T. E., & Nagy, K. L. (1994). Chemical weathering rate laws and global geochemical cycles. *Geochimica et Cosmochimica Acta*, *58*, 2361–2386.

- Le Chat, G., Zaslavsky, A., Meyer-Vernet, N., Issautier, K., Belheouane, S., Pantellini, F., ... Kasper, J. C. (2013). Interplanetary nanodust detection by the Solar Terrestrial Relations Observatory/WAVES low frequency receiver. *Solar Physics*, 286, 549–559.
- Liu, H., Conside, D. B., Horowitz, L. W., Crawford, J. H., Rodriguez, J. M., Strahan, S. E., ... Yantosca, R. M. (2016). Using beryllium-7 to assess cross-tropopause transport in global models. *Atmospheric Chemistry and Physics*, 16, 4641–4659.
- Love, S. G., & Brownlee, D. E. (1991). Heating and thermal transformation of micrometeoroids entering the Earth's atmosphere. *Icarus*, 89, 26–43.
- Love, S. G., & Brownlee, D. E. (1993). A direct measurements of the terrestrial mass accretion rate of cosmic dust. *Science*, 262, 550–553.
- Mann, G. W., Carslaw, K. S., Spracklen, D. V., Ridley, D. A., Manktelow, P. T., Chipperfield, M. P., ... Johnson, C. E. (2010). Description and evaluation of GLOMAP-mode: A modal global aerosol microphysics model for the UKCA composition-climate model. *Geoscientific Model Development*, 3, 519–551.
- Marcantonio, F., Turekian, K. K., Higgins, S., Anderson, R. F., Stute, M., & Schlosser, P. (1999). The accretion rate of extraterrestrial ³He based on oceanic ²³⁰Th flux and the relation to Os isotope variation over the past 200,000 years in an Indian Ocean core. *Earth and Planetary Science Letters*, 170, 157–168.
- Marsh, D. R., Janches, D., Feng, W., & Plane, J. M. C. (2013). A global model of meteoric sodium. *Journal of Geophysical Research: Atmospheres*, 118, 11,442–11,452. <https://doi.org/10.1002/jgrd.50870>
- Marsh, D. R., Mills, M. J., Kinnison, D. E., Lamarque, J. F., Calvo, N., & Polvani, L. M. (2013). Climate change from 1850 to 2005 simulated in CESM1(WACCM). *Journal of Climate*, 26, 7372–7391.
- Mathews, J. D., Janches, D., Meisel, D. D., & Zhou, Q. H. (2001). The micrometeoroid mass flux into the upper atmosphere: Arecibo results and a comparison with prior estimates. *Geophysical Research Letters*, 28, 1929–1932. <https://doi.org/10.1029/2000GL012621>
- Maurette, M., Hammer, C., Brownlee, D. E., Reeh, N., & Thomsen, H. H. (1986). Placers of cosmic dust in the blue ice lakes of Greenland. *Science*, 233, 869–872.
- Miller, Y., Gerber, R. B., & Vaida, V. (2007). Photodissociation yields for vibrationally excited states of sulfuric acid under atmospheric conditions. *Geophysical Research Letters*, 34, L16820. <https://doi.org/10.1029/2007GL030529>
- Mills, M. J., Schmidt, A., Easter, R., Solomon, S., Kinnison, D. E., Ghan, S. J., ... Gettelman, A. (2016). Global volcanic aerosol properties derived from emissions, 1990–2014, using CESM1 (WACCM). *Journal of Geophysical Research: Atmospheres*, 121, 2332–2348. <https://doi.org/10.1002/2015JD024290>
- Molleker, S., Borrmann, S., Schlager, H., Luo, B., Frey, W., Klingebiel, M., ... Cairo, F. (2014). Microphysical properties of synoptic-scale polar stratospheric clouds: In situ measurements of unexpectedly large HNO₃-containing particles in the Arctic vortex. *Atmospheric Chemistry and Physics*, 14, 10,785–10,801.
- Morgenstern, O., Braesicke, P., O'Connor, F. M., Bushell, A. C., Johnson, C. E., Osprey, S. M., & Pyle, J. A. (2009). Evaluation of the new UKCA climate-composition model—Part 1: The stratosphere. *Geoscientific Model Development*, 2, 43–57.
- Nesvorný, D., Jenniskens, P., Levison, H. F., Bottke, W. F., Vokrouhlický, D., & Gounelle, M. (2010). Cometary origin of the zodiacal cloud and carbonaceous micrometeorites. Implications for hot debris disks. *The Astrophysical Journal*, 713, 816–836.
- Patterson, D. B., & Farley, K. A. (1998). Extraterrestrial ³He in seafloor sediments: Evidence for correlated 100 kyr periodicity in the accretion rate of interplanetary dust, orbital parameters, and Quaternary climate. *Geochimica et Cosmochimica Acta*, 62, 3669–3682.
- Pedatella, N. M., Raeder, K., Anderson, J. L., & Liu, H. L. (2013). Application of data assimilation in the Whole Atmosphere Community Climate Model to the study of day-to-day variability in the middle and upper atmosphere. *Geophysical Research Letters*, 40, 4469–4474. <https://doi.org/10.1002/grl.50884>
- Pedatella, N. M., Raeder, K., Anderson, J. L., & Liu, H. L. (2014). Ensemble data assimilation in the Whole Atmosphere Community Climate Model. *Journal of Geophysical Research: Atmospheres*, 119, 9793–9809. <https://doi.org/10.1002/2014JD021776>
- Petit, J. R., Jouzel, J., Raynaud, D., Barkov, N. I., Barnola, J. M., Basile, I., ... Stievenard, M. (1999). Climate and atmospheric history of the past 420,000 years from the Vostok ice core, Antarctica. *Nature*, 399, 429–436.
- Peucker-Ehrenbrink, B., & Ravizza, G. (2000). The effects of sampling artifacts on cosmic dust flux estimates: A reevaluation of nonvolatile tracers (Os, Ir). *Geochimica et Cosmochimica Acta*, 64, 1965–1970.
- Plane, J. M. C. (2012). Cosmic dust in the Earth's atmosphere. *Chemical Society Reviews*, 41, 6507–6518.
- Plane, J. M. C., Feng, W., & Dawkins, E. C. (2015). The mesosphere and metals: Chemistry and changes. *Chemical Reviews*, 115, 4497–4541.
- Prasad, M. S., Rudraswami, N. G., & Panda, D. K. (2013). Micrometeorite flux on Earth during the last ~50,000 years. *Journal of Geophysical Research: Planets*, 118, 2381–2399. <https://doi.org/10.1002/2013JE004460>
- Rienecker, M. M., Suarez, M. J., Gelaro, R., Todling, R., Bacmeister, J., Liu, E., ... Woollen, J. (2011). MERRA: NASA's Modern-Era Retrospective Analysis for Research and Applications. *Journal of Climate*, 24, 3624–3648.
- Saunders, R. W., Dhomse, S., Tian, W. S., Chipperfield, M. P., & Plane, J. M. C. (2012). Interactions of meteoric smoke particles with sulphuric acid in the Earth's stratosphere. *Atmospheric Chemistry and Physics*, 12, 4387–4398.
- Saunders, R. W., & Plane, J. M. C. (2006). A laboratory study of meteor smoke analogues: Composition, optical properties and growth kinetics. *Journal of Atmospheric and Solar- Terrestrial Physics*, 68, 2182–2202.
- Saunders, R. W., & Plane, J. M. C. (2010). The formation and growth of Fe₂O₃ nanoparticles from the photo-oxidation of iron pentacarbonyl. *Journal of Aerosol Science*, 41, 475–489.
- Saunders, R. W., & Plane, J. M. C. (2011). A photo-chemical method for the production of olivine nanoparticles as cosmic dust analogues. *Icarus*, 212, 373–382.
- Schippers, P., Meyer-Vernet, N., Lecacheux, A., Kurth, W. S., Mitchell, D. G., & André, N. (2014). Nanodust detection near 1 AU from spectral analysis of Cassini/Radio and Plasma Wave Science data. *Geophysical Research Letters*, 41, 5382–5388. <https://doi.org/10.1002/2014GL060566>
- Soyol-Erdene, T. O., Huh, Y., Hong, S., & Do Hur, S. (2011). A 50-year record of platinum, iridium, and rhodium in Antarctic snow: Volcanic and anthropogenic sources. *Environmental Science and Technology*, 45, 5929–5935.
- Steel, D. I., Asher, D. J., & Clube, S. V. M. (1991). The structure and evolution of the Taurid complex. *Monthly Notices of the Royal Astronomical Society*, 251, 632–648.
- Stevenson, D. S., Dentener, F. J., Schultz, M. G., Ellingsen, K., van Noije, T. P. C., Wild, O., ... Szopa, S. (2006). Multimodel ensemble simulations of present-day and near-future tropospheric ozone. *Journal of Geophysical Research*, 111, D08301. <https://doi.org/10.1029/2005JD006338>
- Suavet, C., Gattacceca, J., Rochette, P., Perchiazzi, N., Folco, L., Duprat, J., & Harvey, R. P. (2009). Magnetic properties of micrometeorites. *Journal of Geophysical Research*, 114, B04102. <https://doi.org/10.1029/2008JB005831>
- Subasinghe, D., Campbell-Brown, M. D., & Stokan, E. (2016). Physical characteristics of faint meteors by light curve and high-resolution observations, and the implications for parent bodies. *Monthly Notices of the Royal Astronomical Society*, 457, 1289–1298.
- Taylor, S., Lever, J. H., & Harvey, R. P. (1998). Accretion rate of cosmic spherules measured at the South Pole. *Nature*, 392, 899–903.

- Thordarson, T., & Larsen, G. (2007). Volcanism in Iceland in historical time: Volcano types, eruption styles and eruptive history. *Journal of Geodynamics*, 43, 118–152.
- Toppani, A., Libourel, G., Engrand, C., & Maurette, M. (2001). Experimental simulation of atmospheric entry of micrometeorites. *Meteoritics and Planetary Science*, 36, 1377–1396.
- Voigt, C., Schlager, H., Luo, B. P., Dornbrack, A. D., Roiger, A., Stock, P., ... Peter, T. (2005). Nitric acid trihydrate (NAT) formation at low NAT supersaturation in polar stratospheric clouds (PSCs). *Atmospheric Chemistry and Physics*, 5, 1371–1380.
- Vondrak, T., Plane, J. M. C., Broadley, S., & Janches, D. (2008). A chemical model of meteoric ablation. *Atmospheric Chemistry and Physics*, 8, 7015–7031.
- Winckler, G., Anderson, R. F., Stute, M., & Schlosser, P. (2004). Does interplanetary dust control 100 kyr glacial cycles? *Quaternary Science Reviews*, 23, 1873–1878.
- Winckler, G., & Fischer, H. (2006). 30,000 years of cosmic dust in Antarctic ice. *Science*, 313, 491–491.
- Wogelius, R. A., & Walther, J. V. (1992). Olivine dissolution kinetics at near-surface conditions. *Chemical Geology*, 97, 101–112.
- Wolff, E. W., Barbante, C., Becagli, S., Bigler, M., Boutron, C. F., Castellano, E., ... Wegner, A. (2010). Changes in environment over the last 800,000 years from chemical analysis of the EPICA Dome C ice core. *Quaternary Science Reviews*, 29, 285–295.
- Wolff, E. W., Bigler, M., Curran, M. A. J., Dibb, J. E., Frey, M. M., Legrand, M., & McConnell, J. R. (2012). The Carrington event not observed in most ice core nitrate records. *Geophysical Research Letters*, 39, L08503. <https://doi.org/10.1029/2012GL051603>
- Yudovskaya, M. A., Tessalina, S., Distler, V. V., Chaplygin, I. V., Chugaev, A. V., & Dikov, Y. P. (2008). Behavior of highly-siderophile elements during magma degassing: A case study at the Kudryavy volcano. *Chemical Geology*, 248, 318–341.
- Zanchettin, D., Khodri, M., Timmreck, C., Toohey, M., Schmidt, A., Gerber, E. P., ... Tummon, F. (2016). The Model Intercomparison Project on the climatic response to Volcanic forcing (VolMIP): Experimental design and forcing input data for CMP6. *Geoscientific Model Development*, 9, 2701–2719.
- Zhang, L. M., & Brook, J. R. (2001). The effect of subgrid velocity scale on site-specific/subgrid area and grid-averaged dry deposition velocities. *Atmospheric Environment*, 35, 3841–3850.
- Zhang, J. K., Tian, W. S., Chipperfield, M. P., Xie, F., & Huang, J. L. (2016). Persistent shift of the Arctic polar vortex towards the Eurasian continent in recent decades. *Nature Climate Change*, 6, 1094–1099.